Micromachining of $SrTiO_3$ steps for high-T_c step edge junction dc SQUIDs

INSTITUTE OF PHYSICS PUBLISHING JOURNAL OF MICROMECHANICS AND MICROENGINEERING

J. Micromech. Microeng. **14** (2004) 1–5 PII: S0960-1317(04)53895-0

Micromachining of $SrTiO_3$ steps for high-T_c step edge junction dc SQUIDs

Jing Wang[1], Bing Han[1], Genghua Chen[1], Fengzhi Xu[1], Qiansheng Yang[1] and Tianhong Cui[2]

[1] Institute of Physics and Center for Condensed Matter Physics, Chinese Academy of Sciences, Beijing 100080, People's Republic of China
[2] Institute for Micromanufacturing, Louisiana Tech University, Ruston, LA 71272, USA

E-mail: jwa009@mail.latech.edu

Received 24 September 2002, in final form 18 July 2003
Published 18 August 2003
Online at stacks.iop.org/JMM/14/1 (DOI: 10.1088/0960-1317/14/1/301)

Abstract

In this paper, we establish a model of the micromachined $SrTiO_3$ substrate steps for high-T_c direct-current (dc) superconducting quantum interference devices (SQUIDs). The step angle is determined by the local ion milling rate and re-deposition rate, which is caused by back sputtering of ion milling. At dynamic balance, the maximum possible step angle is predicted to be 75° with an ion beam incidence angle of 45°, which agrees well with the measured value of 71°. In order to obtain a better step sidewall profile, we consider the influences of Nb metal mask micromachining. To avoid a rounded angle at the step upper corner, the minimum thickness of the Nb mask should be 440 nm when the desired step height is 300 nm. At optimized process conditions, steps with sharp, steep angles, and flawless profiles have been fabricated. Nine of the twelve dc SQUIDs thus obtained exhibited resistively shunted junction current–voltage behavior and magnetic field modulation at 77 K.

1. Introduction

Since the advent of high-temperature critical transition (high-T_c) superconductors [1], interference devices based on Josephson junctions have been developed quickly [2, 3]. In order to obtain better resolution, Josephson junctions have evolved from natural grain junctions to bi-crystal junctions [4], bi-epitaxial junctions [5], step edge junctions [6], and other man-made controllable grain junctions [7]. Compared with other high-T_c man-made grain boundary junctions (GBJs), the step edge junction (SEJ) has advantages such as structure simplicity, low cost, and little topographic limitation. However, the step fabrication process, to date, still suffers from the problem of low reproducibility due to the tricky conditions for high step angles. Therefore, an understanding of the micromachining process is necessary. On the other hand, in order to ensure the formation of the grain boundary, the angle of the step edge should be high enough [8–10]. As illustrated in figure 1, there are two edges in a high-T_c Josephson SEJ. At the upper and lower step edges, the 90° grain boundaries (GBs) are both formed due to epitaxial growth. The GBs of step edges behave like Josephson junctions, although the structures are different from those of the classical low-temperature SNS or SIS junctions. If the step angles range from 45° to 60°, both the upper and lower step edges are (103) (103) grain boundaries. These two junctions are in series when $YBa_2Cu_3O_{7-x}$ (YBCO) superconducting film is epitaxially grown on the substrate. If the step angles are larger than 60°, the grain boundaries are no longer symmetric. The upper step edge is the (103) (103) boundary while the lower step edge is the (001) (010) boundary [11]. Because the lower boundary is much weaker than the upper one, the total junction behaves as if only the lower boundary exists [12]. In order to seek lower device noise, a high step angle is necessary due to its single boundary characteristics.

To pursue the high reproducibility and the high step angle, a model of micromachined step substrates for direct-current (dc) superconducting quantum interference devices (SQUIDs) has been established, with which we can predict the highest possible step angle as well as better control of the fabrication process. In order to obtain a sharp step sidewall, we also consider the influences of

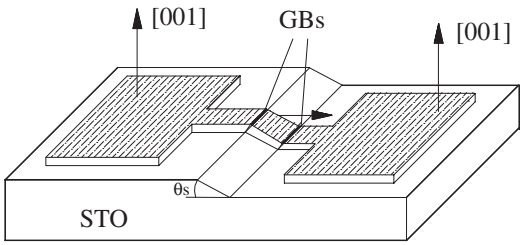

Figure 1. Diagram of high-T_c Josephson SEJ; two GBs are formed at the upper and lower step edges.

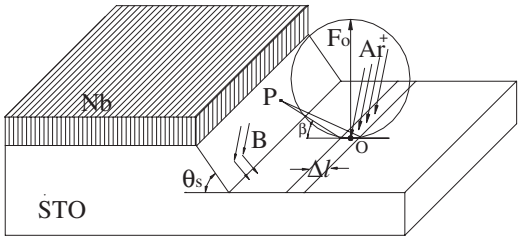

Figure 2. Ar^+ milling process with substrate half covered with Nb mask; the sidewall milling (point B) and re-deposition effect (point *P*) reaches a dynamic balance.

processing conditions and the choice of the metal mask thickness.

2. Descriptions of micromachining modeling

The most commonly used single-crystal substrates for YBCO superconducting films are $LaAlO_3$ and $SrTiO_3$ (STO). The former has better high-frequency response while the latter has a better crystal structure match. Here, only the STO substrate is discussed because dc SQUIDs are mainly functional at low frequency. When choosing a metal mask for step etching, there are two considerations: the metal should be as hard as possible, and the metal should be removable from the substrate so as not to influence the growth of YBCO superconducting film thereafter. Carbon film is one popularly used mask film, but it is difficult to remove thoroughly. Other frequently used metal masks, such as Ti and Cr, were not suitable here because their etchant would attack and hurt STO heavily. Nb was selected as the metal mask for convenience, although other choices were also reasonable [13].

Our micromachining modeling is in two parts. The first part concerns the step angle. When Nb masks have a perfect profile and height, the sidewall angles are determined by both micromilling at step sidewall and the re-deposition of STO from unprotected areas nearby. The highest angle, which occurs at the highest etching rate, is defined by the dynamic balance of both processes. The second part of the modeling concerns the sidewall profile. The profiles of Nb masks will influence the STO sidewall by transferring their structures. Also, the thicknesses of the masks should be high enough to prevent roundness at the step upper corners due to mask recession. Both the profile influences and the choice of the minimum mask thickness will be discussed later.

3. Analysis on high step angles

As shown in figure 2, the micromachining process of the step sidewall is composed of two processes: milling (illustrated at point B) and re-deposition (illustrated at point P). For the half unshielded plane, the milling rate V_{plane} is the function of incidence angle α, which is defined as the angle between incidence ion beam and the normal of the plane. The milling rate at the step sidewall V_{slope} obeys the same rule as V_{plane} except for the difference of incidence angle. The re-deposition rate V_{D} is mainly determined by the sputtering yield from the unshielded plane. The highest angle is formed when these two processes reach a balance.

3.1. Re-deposition rate and milling rate at step sidewall

As illustrated in figure 2, the strip Δl at the arbitrary point O of the unshielded plane has a distance d to the slope at point P. The open angle between OP and the bed of the step is β. If the maximum flux of back sputtering by ion milling is F_{o}, the sputtering material f_β in the β direction is

$$f_\beta = F_{\text{o}} \cdot \cos\left(\frac{\pi}{2} - \beta\right) = F_{\text{o}} \cdot \sin\beta \tag{1}$$

Because the energy of the back sputtered material is low, it is reasonable to assume that all the sputtered material is re-deposited on the surface without a second sputtering. Thus, the deposited material at point *P* received from strip Δl is

$$f(p) = F_{\text{o}} \cdot \sin\beta \cdot \sin(\theta_{\text{s}} - \beta) \cdot \Delta l/d \tag{2}$$

where θ_{s} is the step angle.

Equation (2) describes the re-deposited material flux caused by the sputtered material. The re-deposited material at point *P* received from strip Δl, which is located on the step bed area, is proportional to the maximum back sputtering flux F_{o} and the width of strip Δl and is inversely proportional to the distance d. Considering $\Delta l = d \cdot (-\Delta\beta)/\sin\beta$, equation (2) can be rewritten as

$$f(p) = -F_{\text{o}} \cdot \sin(\theta_{\text{s}} - \beta)\Delta\beta \tag{3}$$

Integrating all possible β values at the step bed area, the total re-deposited material at point *P* is

$$F(p) = \int_{\theta_{\text{s}}}^{0} -F_{\text{o}} \cdot \sin(\theta_{\text{s}} - \beta) \cdot \Delta\beta = F_{\text{o}}(1 - \cos\theta_{\text{s}}) \tag{4}$$

Because the re-deposition rate V_{D} is proportional to the deposition flux $F(p)$, the deposition rate is

$$V_{\text{D}} = A(1 - \cos\theta_{\text{s}}) \tag{5}$$

where A is a constant, which can be determined by the boundary conditions. If there exists an infinite plane covering the step bed, which corresponds to the step angle $\theta_{\text{s}} = \pi$, then all the sputtered material is deposited onto this plane. The deposition rate is then equal to the milling rate V_{plane}. From $V_{\text{D}} = V_{\text{plane}} = A(1 - \cos\pi) = 2A$, the re-deposition rate, which is related to the step angle and the milling rate at the unshielded plane, can be obtained as

$$V_{\text{D}} = \frac{V_{\text{plane}}}{2}(1 - \cos\theta_{\text{s}}) \tag{6}$$

The derivation of the milling rate is simpler because it follows the same rule as the plane milling except for a different incident angle. If the incident angle of the ion beam at half unshielded plane is α and the incidence angle at the step slope

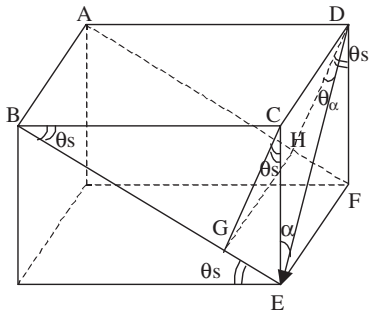

Figure 3. Relations of bed incidence angle α, step angle θ_s and step incidence angle θ_α.

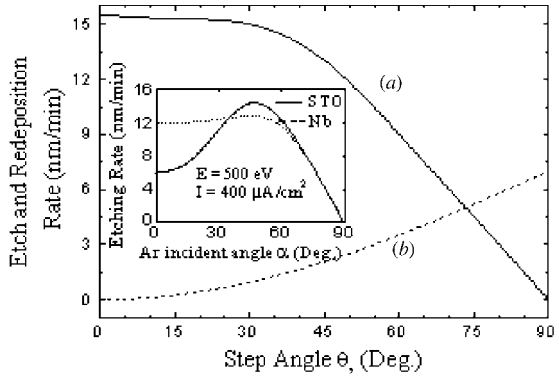

Figure 4. The inset shows the etching rule of STO and Nb mask. The incident angle is chosen as 45° where the highest ratio of STO/Nb is acquired. The milling rate shown by curve (*a*) equals the re-deposition rate shown in curve (*b*) at the highest possible step angle of 75°.

is θ_α, the relations of α, θ_α and step angle θ_s are illustrated in figure 3. Section DE represents the incidence ion beam trajectory. Plane ABEF is the step slope plane and plane CGHD is the normal plane of the step slope. In pyramid DFEH, there exists $DH = DE \cdot \cos\theta_\alpha = ED \cdot \cos\alpha \cdot \cos\theta_s$. The relation of α and θ_α is then $\cos\theta_\alpha = \cos\alpha \cdot \cos\theta_s$. Although it cannot be formularized, the milling rule as a function of the incidence angle can be obtained from the experimental curve. From the data in the inset of figure 4, where the solid and dotted lines are curves for STO and Nb milling rate respectively, the milling rate of the step slope dependent on θ_s can be derived easily if the incident angle α remains constant.

3.2. Highest possible step angle at dynamic balance condition

In order to obtain a higher step angle, the ion beam should be chosen at an incidence angle where the ratio of substrate milling to metal mask milling is the highest. This can be found when the incidence angle α is about 45° (as shown in the inset of figure 4). When the incidence angle is fixed at 45°, the etching rate of the step slope can be derived as curve (*a*) in figure 4. The re-deposition rate determined by equation (6) is plotted as curve (*b*). The cross point of these two curves corresponds to the step angle of 75°, which is the highest possible angle we can obtain. The physical image of micromilling is as follows. If the step angle is larger than 75°, the re-deposition rate is larger than the milling rate. There will be more material accumulated at step slope than etched. Thus the step angle becomes smaller. In contrast, if the step angle is smaller than 75°, the etched material competes over the accumulated material. The step angle will then become larger. This dynamic balance keeps the step angle constant. The highest possible step angle is 75° when the incident angle α is kept at 45°.

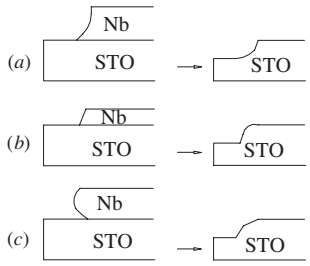

Figure 5. Illustration of the influence of the metal mask profile on step angle: (*a*) low mask angle causes low step angle; (*b*) thin mask layer causes up round corner; (*c*) undercut of mask film causes small section on step profile.

4. Analysis on step sidewall profile

Unlike radio-frequency (rf) SQUIDs, which only have one junction, dc SQUIDs are comprised of two shunted junctions. In addition, these two junctions must be exactly the same so as to obtain the symmetric interference effect. This is why most junctions in dc SQUIDs are patterned as close as possible to keep the junction parameters identical. Because of the above requirements, the step bank line needs to be long enough to accommodate two junctions and consistent enough to keep these two junctions the same.

The profile of step sidewall is primarily determined by the profile of the Nb mask film. Using atomic force microscopy (AFM), we analyze several influences of mask and micromilling conditions on the step profile.

4.1. Influences of mask profile on step sidewall profile

In order to obtain a better step profile, the milling of the metal mask should also be taken into account. If the Nb film has a slight slope, the low angle of the mask will be transferred to the substrate due to the milling of the mask film. The upper angle of the obtained step slope is relatively high, but the lower angle is relatively low (as shown in figure 5(*a*)). If the Nb mask is undercut, the upper edge of the obtained step will incur a section because of the recession of the mask (as shown in figure 5(*c*)). If the thickness of the metal mask is thin, even for an Nb mask with a sharp and steep original profile, the upper corner of the step will be rounded owing to the milling of the mask (as shown in figure 5(*b*)). Actually, the steep Nb mask can be easily obtained by controlling the etching time of the reactive ion etching. Only the minimum thickness of Nb mask should be found.

4.2. Metal mask thickness chosen

The micromachining process of Nb etching is illustrated in figure 6. The *x*- and *y*-axes denote the surface and sidewall

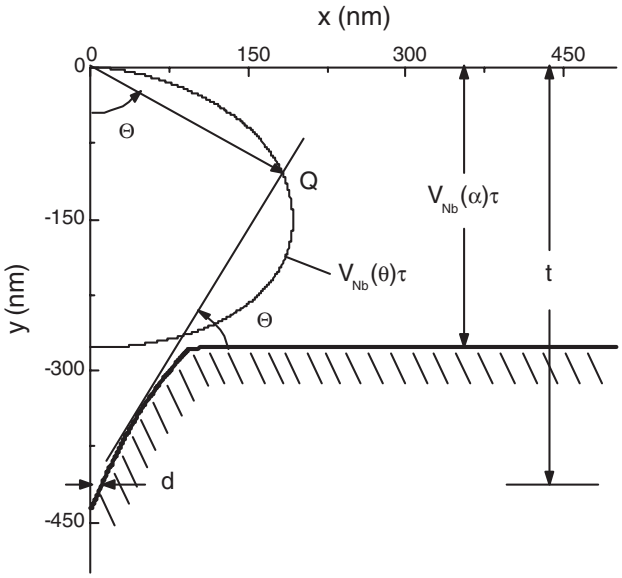

Figure 6. Illustration of Nb mask recession because of micromilling. After a period of time τ, the minimum mask thickness t is 440 nm if the recession value d is zero.

of the original Nb mask film. For a period of etching time τ, which is determined by the necessary step height, the Nb mask is etched by a thickness of $V_{\mathrm{Nb}}(\alpha)\tau$, where α is the incidence angle of 45°. For the Nb sidewall, the incidence angle of the milling beam is different and thus the milling rate is different at different directions. At direction Θ, the etching vector is OQ, whose length is equal to $V_{\mathrm{Nb}}(\theta)\tau$, where $V_{\mathrm{Nb}}(\theta)$ is the milling rate and θ is the incident angle at the Nb sidewall. Similar to the analysis above, there is the relation $\cos\theta = \cos\alpha \cdot \cos\Theta$. The line perpendicular to OQ denotes the front etching plane at direction Θ and it is tangent to the final profile of the Nb surface. From the Nb milling data obtained in the inserted picture of figure 4, the trajectory of point Q is defined by the length of $V_{\mathrm{Nb}}(\theta)\tau$ and the direction of Θ is given through the relation of θ, α and Θ. The final Nb profile, shown as the shaded line in figure 6, is obtained by finding the series of OQ tangent lines. The minimum Nb thickness needs to be calculated by considering the recess distance d. If the step height is 300 nm, the minimum thickness t of the Nb film is 440 nm when recess d is exactly equal to zero.

5. Fabrication and results

Before the process, the STO substrates needed to be well cleaned with deionized (DI) water, acetone and IPA until there was no submicrometer dust visible on the surface under microscopy. The substrates were then put into a chamber for metal mask sputtering. The base pressure was less than 5×10^{-3} Pa, the Ar pressure was 3 Pa and the sputtering rate was 800 Å min^{-1} with total Nb film thickness of 440 nm. The mask film was then patterned by photolithography. The developing time needed to be well controlled so that no residue was left at the bed area to affect the following process and no saw-toothed profile arose due to overdevelopment. The following reactive etching by CF_4 gas was performed with a strictly controlled time of 240 s.

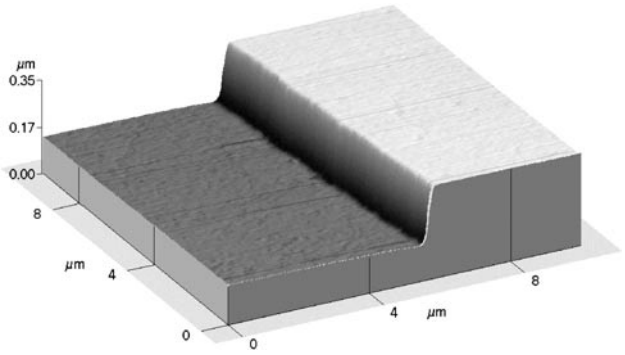

Figure 7. AFM profile of high reproducible micromachining step substrate.

After soaking in acetone to remove photoresist, the substrates were laid into the chamber at such an orientation that the incident angle α was 45°. Our Kaufman-type Ar^+ ion gun had a uniform-current area of 80 mm in diameter. The ion energy was set at 500 eV and the ion beam current density was tuned at 400 μA cm^{-2}. The substrates were thoroughly water-cooled and the final step height aimed at was 250 nm. Later, another reactive etching was performed with thorough Nb film removal. A more detailed description of the processing can be found in [14]. Under such strict ion milling control and optimized metal mask thickness, the high-quality step substrates were fabricated successfully. As shown in figure 7, the upper and lower angles of the step are sharp and smooth. The step angle is about 71°, which is close to the maximum step angle of 75° as described in the modeling. There are no needles, pits, waves, trenches, or other flaws at the surface. Within a 4 μm scope, the step is consistent, which ensures the possibility of single step GBs because the prepared junction width is 3 μm. The bank line of the step is straight, which ensures the identity of two GBs with a distance of about 10 μm.

YBCO superconducting films were deposited on prepared step substrates by pulsed laser deposition (PLD) with a thickness of about 200 nm, which was about 80% of the step height. The current densities of the film without crossing the steps were measured with a value of 5.2×10^6 A cm^{-2} at 77 K. The two shunted junctions located at the same wall of the steps were patterned by photolithography and dry etching. Finally, dc SQUID characteristics were measured at liquid nitrogen temperature in a magnet shield system, with an environment magnetic field of less than 0.5 nT.

A well-performed Josephson junction does not necessarily guarantee a good-quality dc SQUID because identical properties of the shunted junctions are required. This is why the characteristics of dc SQUIDs instead of single junctions are presented here. One typical current–voltage (I–V) curve of the fabricated dc SQUIDs at 77 K is plotted in figure 8. The small increase slightly above I_C agrees with the description of the resistively shunted junction (RSJ) model. At higher voltages, the I–V curve approaches an ohmic line, $V = I_C R_N$. Here, normal resistance R_N is about 1.04 Ω, in accordance with the RSJ model also. The SQUID critical current $2I_C$ is about 140 μA, which gives a current density of $J_C \sim 10^4$ A cm^{-2}, two orders of magnitude lower than that in the bulk area. The inset of figure 8 shows the voltage verse

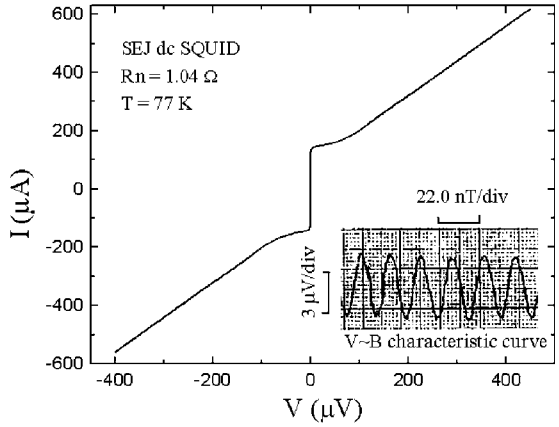

Figure 8. *I–V* characteristic plot of SEJ dc SQUID shows RSJ behavior. The inset is the magnetic modulation curve. Both are obtained at liquid nitrogen temperature.

magnetron field characteristic (*V–B*) curve. Calculated from the Seed theory [15], the modulated voltage ΔV is about 5 μV, in reasonable agreement with the value measured at 77 K.

Twelve step substrates were prepared and YBCO film dc SQUIDs were fabricated in the same conditions. Triangular waves of SQUIDs at 77 K were inspected, which functioned as the criteria for device producibility. Nine of the twelve dc SQUIDs exhibited RSJ behavior and voltage modulations depending on the applied magnetic field. The strict controls of the milling conditions and the optimized mask thickness have made the micromachining method for Josephson junction step substrate fabrication a highly reproducible process.

6. Conclusions

In this paper we have presented the micromachining process of ion milling for a Josephson step edge junction. The step angle is determined by the dynamic balance between the ion beam milling and the re-deposition rate of back sputtering at the sidewall. The milling rate at the step sidewall can be derived from experimental data, and the re-deposition rate was derived as $V_D = \frac{V_{plane}}{2}(1 - \cos\theta_s)$. At an ion beam incidence angle of 45°, the dynamic balanced process caused a maximum possible step angle of 75°, which agreed well with the measured value of 71°.

An ideal step sidewall profile needs good control of the metal mask profile and a proper thickness. The recess distance of the Nb mask was checked and calculated. In order to avoid the rounded angle at the upper step corner, the metal mask should be thicker than 440 nm when the intended step height is 300 nm.

The fabricated step substrates had a sharp and steep step angle and flawless profile. Nine of the twelve fabricated dc SQUIDs exhibited voltage modulations at liquid nitrogen temperature.

Acknowledgments

This work was supported by the National Center for R&D on Superconductivity and the Ministry of Science and Technology of China (NKBRSF-G19990646).

References

[1] Bednorz J G and Muller K A 1986 Possible high T_C superconductivity in the Be–La–Cu–O system *Z. Phys.* B **64** 189–4

[2] Mozhaev, Peter B, Borisenko, Igor V, Ovsyannikov, Elena G, Ovsyannikov and Gennady A 2002 High-temperature superconducting bi-crystal Josephson junctions with asymmetric current biasing: The DC-SQUID configuration *Physica* C **372–376** 150–3

[3] Amin M H S, Omelyanchouk A N and Zagoskin A M 2002 DC SQUID based on the mesoscopic multiterminal Josephson junction *Physica* C **372–376** 178–2

[4] Dimos D, Chaudhari P, Mannhart J and LeGoues F K 1988 Orientation dependence of grain-boundary critical currents in $YBa_2Cu_3O_7$-delta bicrystals *Phys. Rev. Lett.* **61** 219–3

[5] Char K, Colclough M S, Garrison S M, Newman N and Zaharchuk G 1991 Bi-epitaxial grain boundary junctions in $YBa_2Cu_3O_7$ *Appl. Phys. Lett.* **59** 733–2

[6] Daly K P, Dozier W D, Burch J F, Coons S B, Hu R, Platt C E and Simon R W 1991 Substrate step-edge $YBa_2Cu_3O_7$ rf SQUIDs *Appl. Phys. Lett.* **58** 543–3

[7] Di Iorio M S, Yoshizumi S, Yang K-Y, Zhang J and Maung M 1991 Practical high T_C Josephson junctions and dc SQUIDs operating above 85 K *Appl. Phys. Lett.* **58** 2552–3

[8] Jia C L, Kabius B and Herrmann K 1991 Microstructure of epitaxial $YBa_2Cu_3O_7$ films on step-edge $SrTiO_3$ substrates *Physica* C **175** 545–5

[9] Herrmann K, Zhang Y, Muck H-M, Schubert J, Zander W and Braginski A I 1991 Characterization of $YBa_2Cu_3O_7$ step-edge Josephson junctions *Supercond. Sci. Technol.* **4** 583–3

[10] Herrmann K, Kunkel G, Siegel M, Schubert J, Zander W, Braginski A I, Jia C L, Kabius B and Urban K 1995 Correlation of $YBa_2Cu_3O_7$ step-edge junction characteristics with microstructure *J. Appl. Phys.* **78** 1131–8

[11] Koelle D, Kleiner R, Ludwig F, Dantsker E and Clarke J 1999 High-transition-temperature SQUIDs *Rev. Mod. Phys.* **71** 632–46

[12] Jia C L, Kabius B, Urban K, Herrmann K, Schubert J, Zander W and Braginski A I 1992 The microstructure of epitaxial $YBa_2Cu_3O_7$ films on steep steps in $LaAlO_3$ substrates *Physica* C **196** 211–7

[13] Sun J Z, Gallagher W J, Callegari A C, Foglietti V and Koch R H 1993 Improved process for high-T_C superconducting step-edge junctions *Appl. Phys. Lett.* **63** 1561–3

[14] Chen G H, Wang J, Zhao S, Han B and Yang Q S 2001 Analysis of Step Etching on $SrTiO_3$ Substrates for the step-edge YBCO Josephson junctions *Chin. Phys. Lett.* **18** 106–4

[15] Seed R G, Dorsey P C, How H, Widom A and Vittoria C 1994 Planar superconducting YBCO microwave mixer employing an engineered grain boundary weak link junction *IEEE Trans. Appl. Supercond.* **4** 149–6